The Impact of Structural Deformations on the Performance of Li-ion Insertion Hosts

Jessica L. Andrews,[†] Michael J. Brady,[†] Eric T. McClure,[†] and Brent C. Melot[*,†,‡]

[†]*Department of Chemistry, University of Southern California, Los Angeles, California 90089, USA*

[‡]*Department of Chemical Engineering and Materials Science, University of Southern California, Los Angeles, California 90089, United States*

E-mail: melot@usc.edu

Abstract

Over the course of more than three decades, Li-ion batteries have come to revolutionize the way we store and transport energy. These incredibly compact electrochemical devices rely fundamentally on the ability to reversibly insert lithium ions into densely packed arrangements of atoms. Of the tens of thousands of materials reported in the structural databases, only a very small number have been shown to be capable of accommodating the kind of fast ionic diffusion necessary to operate in practical devices. In honor of John B. Goodenough's 100^{th} birthday, this perspective will overview the current understanding of the kinds of structural features that help and/or hurt fast lithium ion transport through insertion hosts, with a particular focus on the role that the rotation of rigid subunits plays in the movement of lithium through the solid state.

Introduction

It would be no exaggeration to say that the development of the Li-ion battery was the watershed moment that propelled the field of portable energy storage to what it is today. Underpinning this paradigm-shifting technology is the ability to move charged ions into and out of materials without destroying their crystalline structure, allowing for highly efficient and reversible (dis)charge cycles. While a great number of groups reported pivotal pieces of information that ultimately allowed these devices to become reality,[1–13] it was arguably the first report on $LiCoO_2$ by John B. Goodenough and co-workers in 1980 that highlighted their true potential.[14]

Since that seminal work, Li-ion batteries have come to dominate energy storage for consumer products because of their light weight, large operating potentials, and slow self-discharge rates.[15] Despite the massive body of work studying Li-ion insertion hosts, many questions still remain about how to develop new materials that can match or exceed the performance of the rock salt family. In a previous report, we discussed how the local structure and character of the chemical bonds influence the operating voltages;[16] this perspective will instead examine how the distortions that crystal structures experience during the (de)insertion of lithium ions impact the rate performance and reversibility of the electrode material.

This perspective will begin with a brief overview of distortions seen in oxide-based electrodes and contrast this against more compositionally complex polyanionic hosts. This will be followed with the presentation of a generalized method that utilizes symmetry-adapted representational analysis to characterize the reversibility of these atomic rearrangements. We will conclude by discussing a handful of examples from the literature where elucidating the nature of these distortions significantly enhanced the community's understanding of the electrochemical performance.

The current state-of-the-art positive electrodes in Li-ion batteries rely on $LiCoO_2$,[14] $LiNi_{1/3}Co_{1/3}Mn_{1/3}O_2$,[17] $LiNi_{0.70}Co_{0.15}Al_{0.15}O_2$,[18] or $LiMn_2O_4$,[19] some of which are illustrated in Figure 1. The common structural feature in these compounds is the presence of channels that allow for easy movement of ions and, naively, may allow materials to be cycled with minimal change to the host framework. This void space typically results from a layered topology (as in $LiCoO_2$) or from a coherent network of empty interstices within a close-packed anionic lattice (as in $LiMn_2O_4$). Importantly, not all empty space within a structure will be capable of facilitating ionic transport. For example, ionic conduction through meso- or micro-pores in a

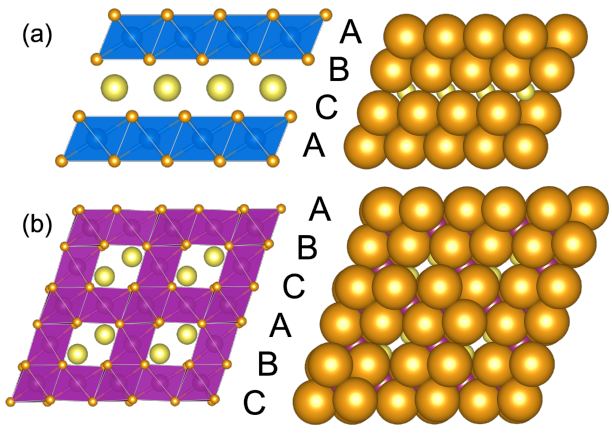

Figure 1: Illustration of the polyhedral and close-packed representations of $LiCoO_2$ (a) and $LiMn_2O_4$ (b) where lithium are shown in yellow while the transition-metal polyhedra for cobalt and manganese are shown in blue and purple, respectively, and are coordinated by oxygen in orange.

material typically requires the incorporation of confined electrolyte solution into the pore in order to observe fast diffusion.[20–22] This suggests a "Goldilocks" situation where the interstitial space needs to be "just right" to solvate the alkali ions within the structure without binding them so tightly that they cannot diffuse under applied fields.

Following the advent of oxide-based hosts, the field soon turned its attention towards the far more diverse family of polyanionic compounds. Polyanionic materials are characterized by the presence of complex oxoanionic subunits that exhibit rigid covalent bonds between a main group element and its surrounding ligands. Because of the many ways these polyhedra can pack, they offer a huge number of unique structural topologies that can be explored. Masquelier and Croguennec,[23] as well as many others,[24,25] have extensively reviewed the field and summarized the advantages that polyanionic phases offer as follows: (1) Robust structures that provide long-term stability over an extended number of cycles; (2) Inductive effects from polyanionic groups provide a route to enhance redox potentials; (3) Versatile frameworks that allow for rich compositional phase diagrams and simple chemical substitutions.

These phases also offer advantages over oxides because the strong bonding between the main group elements and their oxygen ligands provides superior safety characteristics. This is attributed to the fact that polyanionic compounds rarely release O_2 on thermal decomposition, which can exacerbate thermal runaway when cells fail.[23,26] Perhaps more relevant to the structural transformations explored here is the contrast between the rigid (strongly covalent) main group polyhedra and the deformable (more ionic) transition metals. This effectively creates hinges around which polyhedra can pivot during cycling, and will be discussed presently.

Lithium Ion Diffusion through Oxides and Polyanionic Hosts

The classical picture of diffusion through the solid-state depicts the migration of ions between empty interstices or vacancies in the lattice.[27,28] This hopping is strongly influenced by the nature of the bonding in the host framework because of electrostatic interactions that occur between the positively charged alkali ions and the negatively charged anions.[29–31] In layered oxides, the distortions that occur as lithium ions move in and out of a structure trigger substantial changes to the lattice due to the looser packing of the anions. Similarly, the framework of spinel $LiMn_2O_4$ is known to undergo a Jahn–Teller distortion as Mn^{4+} is reduced to Mn^{3+}, which causes an elongation along the c-axis of the cubic cell and lowers the symmetry to the tetragonal polymorph of λ-MnO_2.[32]

As alluded to, polyanionic materials experience significantly different distortions to their frameworks upon (de)lithiation. As an illustration of this type of mechanism, consider the case of tavorite-$LiFeSO_4F$,

which Tarascon and co-workers have studied extensively in both its lithiated and delithiated forms.[33–35] This was possible because the delithiated form (i.e., $FeSO_4F$) can be prepared directly, rather than having to (electro)chemically oxidize the parent, which can often produce biphasic or amorphous materials that are difficult to analyze.[36]

The framework of both phases consists of FeO_4F_2 octahedra that share their corners through fluoride vertices oriented in a *trans* configuration with respect to each other to produce buckled chains (Figure 2a,b). Importantly, all of the oxygen atoms in the structure are bound within SO_4 tetrahedra that connect the chains via shared corners on the FeO_4F_2 octahedra. The simplest way to describe the structure is by considering a stacking of two kinds of layers, which alternate along the direction of the chains. Within an individual layer, the irons are connected through two SO_4 tetrahedra, and the direction of this connection changes from one plane to another, creating a 3D polyanionic network. It should be noted that there is only one fluoride site in both structures and that the Fe–F–Fe bond angle dictates the degree of buckling along the chains.

$FeSO_4F$ crystallizes in the higher symmetry structure and as lithium ions are inserted, the symmetry drops from $C2/c$ to $P\bar{1}$ as the chains of octahedra rotate out-of-phase with each other (Figure 2c,d). As a result, the single iron in the monoclinic cell splits into two independent Wyckoff sites ($1a$ and $1b$) and the two oxygen atoms of the delithiated phase become four sites in triclinic $LiFeSO_4F$, which are all located on the $2i$ Wyckoff position. The lithium ions are positioned within the channels between the chains and are effectively coordinated by one fluorine and two oxygen atoms to form trigonal planar sites. This is reflected in the Fe–F–Fe bond angle which decreases from 145° in $FeSO_4F$ to 129° in $LiFeSO_4F$. One can see that this distortion occurs via a rotation of one Fe octahedra about the F–Fe–F axis such that it falls into registry with the rotation of the other octahedra (see Supporting Information).

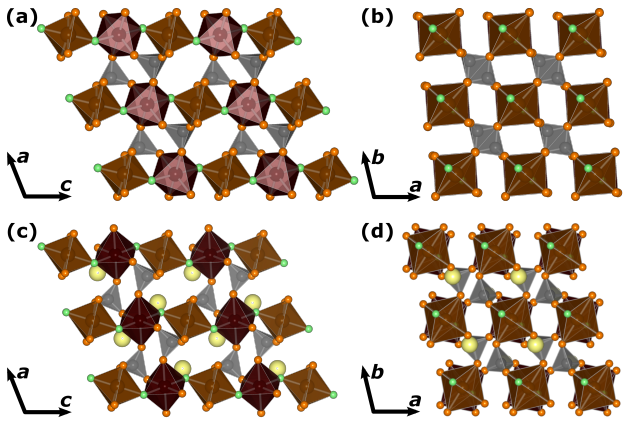

Figure 2: Illustration of differences in the crystal structure of $FeSO_4F$ (a,b) and $LiFeSO_4F$ (c,d). Note that for a more direct comparison, $FeSO_4F$ is illustrated in a tricilinic cell.

Symmetry-Adapted Analysis to Visualize Structural Distortions

Group-theoretical and representational analyses are powerful methods used for understanding crystal structures. They are prominently used to identify the similarities between closely related structures, particularly in describing the perovskite aristotype structure and the diverse bounty of *distorted* perovskites [octahedral rotations, electronic distortions (i.e., first- and second-order Jahn–Teller distortions), site mixing/ordering, etc.].[37–39] More generally, these methods are used for describing structures, phase transitions, chemical changes of materials, and in structure solution/refinement.[33,40–48]

Several tools are available for this type of symmetry-mode analysis, such as the *AMPLIMODES* package from the *Bilbao Crystallographic Server*[49–52] and the *mode decomposition* method in the *ISODISTORT* software from the *ISOTROPY Software Suite.*[53,54] The general procedure is to provide the crystal structures of the pristine and lithiated phases (although with the alkali sites removed), identify the transformation matrix that puts the structures on the same basis, map the atoms between the two structures, and then identify the symmetry modes that displace the atoms between the initial and final positions. When there is a group-subgroup relationship between the structures—as is the case with $Fe_2(MO_4)_3$ (*Pbcn*, #60) and $Li_2Fe_2(MO_4)_3$ ($P2_1/c$, #14), *vide infra*—the transformation matrix is used to transform the high-symmetry structure into the low-symmetry cell. Absent of a group-subgroup relationship, this is further complicated by the need to identify a common subgroup, for which additional tools are available.[51,52,55] The caveat added is that identifying symmetry modes that convert between structures does not mean that they represent the mechanistic path for how structures transform. Rather, this analysis is useful in highlighting how the transformation could occur without a reconstructive phase transformation fracturing the topology of the structure.

Moving Charge through the Solid State

Correlated Polyhedral Rotations

One of the first demonstrations of this group-theoretical analysis applied to Li-ion electrodes was reported by Zhou *et al.* as part of an investigation into $Fe_2(MoO_4)_3$.[56] This anti-NASICON structure consists of corner-connected FeO_6 octahedra and MoO_4 tetrahedra that create several joints around which the polyhedra can rotate as mentioned. In this particular composition, the charge cycling occurs entirely on the $Fe^{3+/2+}$ redox couple, which implies that the MoO_4 tetrahedra are effectively rigid. Perhaps the more interesting aspect of this structure is that it can reversibly accommodate the diffusion of both Li- and Na-ions through its lattice. Yet, while the voltage traces for the insertion of lithium only show a single voltage plateau over a

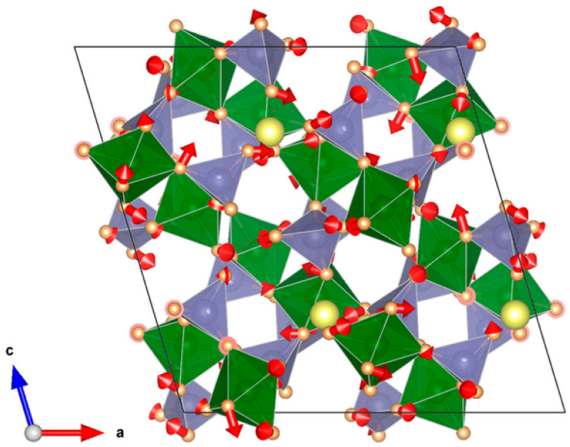

Figure 3: Transformation vectors showing atomic displacements from the symmetry mode analysis between (pristine) $Fe_2(WO_4)_3$ and (lithiated) $Li_2Fe_2(WO_4)_3$. Displacing atoms with the displayed vectors, and inserting lithium atoms at the indicated positions results in the structural description of the lithiated phase. (Iron, tungsten, oxygen, and lithium are shown as green, purple, orange, and yellow, respectively.) [63]

wide composition range (indicating a two-phase insertion process), when cycled against sodium two sloping regions are seen (suggestive of solid-solution behavior). [56,57] Note that care should be taken in comparing two-phase and solid-solution mechanisms as many variables could influence this behavior.

To better understand the contrasting mechanisms, a closer examination of the structure is insightful. Critically, the overall topology of the parent (monoclinic) and lithiated phase (orthorhombic) is unchanged with respect to the polyhedral connectivity (i.e., there is no bond breakage within the framework), so that the transformation occurs exclusively through rotations of the metal subunits. Symmetry mode analysis of the structures shows negligible displacements of the transition-metal ions such that the polyhedral center-of-mass is unchanged. Instead, the displacement vectors are almost entirely associated with the oxygen anions as the polyhedra rotate to accommodate the unit cell volume increase upon lithiation. The sodium intercalation shows a complex evolution of the cell parameters within the same monoclinic structure as the pristine parent. Despite the different space group choice of the lithiated and sodiated structures, the similarity of cell parameters suggests that similar rotations of the polyhedral framework occur in both materials. The main difference is the position of the intercalated ions, which seems to be due to the inherent differences in the size of the two ions.

A natural question that follows is, *what happens when the topology of the framework is maintained, but the metal within the rigid subunits is changed, like in* $Fe_2(WO_4)_3$*?* This phase was first reported by Cheetham and co-workers, [64] and later explored by Goodenough and Manthiram via diffraction of chemically lithiated materials. [65] Since both the pristine and lithiated phases of the two compositions have the same space groups and polyhedral connectivity, it is reasonable to expect that the structures should evolve through

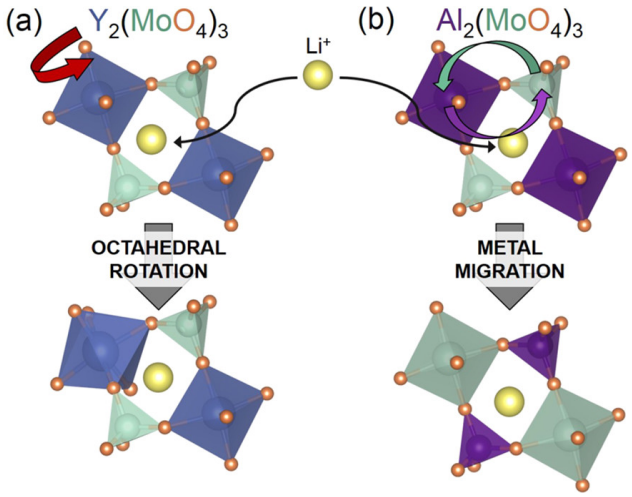

Figure 4: Bonding differences in (a) $Y_2(MoO_4)_3$ and (b) $Al_2(MoO_4)_3$ lead to distinctive structural changes upon lithium intercalation.[66]

very similar polyhedral rotations. The symmetry mode analysis indicated nearly identical changes, but the global distortion amplitudes—the sum of all displacement vectors in the unit cell—is slightly higher in the tungstate (6.50 vs 6.17 Å), depicted visually in Figure 3.[63] These slight differences were attributed to the larger electronegativity (2.36 for W, compared to 2.16 for Mo), which increases the ionicity of the Fe–O bonds through inductive effects and allows for larger displacements of the atoms.

An interesting scenario arises when the redox active element is shifted from the octahedral to tetrahedral site, as in the defect garnet molybdates $A_2(MoO_4)_3$ (A = Al or Y). The phases have the same general formula and nearly identical topology, although the exact tiling of the corner-sharing polyhedra is slightly different. Despite these similarities, the structural deformations during cycling are quite different, leading to highly sloped voltage profiles and rapid capacity fade.[66]

Operando X-ray diffraction (XRD) was used to show that, while the Y-based phase retains the crystallinity of its framework during cycling, the Al analogue rapidly amorphizes. Additional Bragg reflections were not observed during cycling, but X-ray absorption spectroscopy (XAS) revealed substantial changes to the local structure. While the coordination environments in the Y-based phase were effectively maintained, the Al-based phase showed dramatic rearrangements. Combining ^{27}Al NMR with their XAS experiments, Bashian and co-workers determined that both Mo and Al appeared to migrate to new sites within the framework during cycling.[66]

Density functional theory (DFT) calculations were used to postulate that the yttrium ions are bound more tightly within the octahedra due to the covalency of the Y–O bonds, in contrast with the more ionic Al–O bonds, wherein the aluminum ions seem to diffuse through the lattice as a way to relieve some of the local strain. While the metal in the Al-based phase did not appear to mitigate the capacity fade, a

substantial reduction in the voltage polarization was apparent, which suggests that these rearrangements lead to more facile ionic transport. In their study on a related material, Feng *et al.* reported similar observations for $Li_3Cr_2(MoO_4)_3$,[67] which maintains its crystallinity during cycling and exhibits significant polarization and capacity fade. This suggests that distortions of the tetrahedra may generate greater strains within corner-sharing networks that ultimately lead to more complex atomic rearrangements in response to (de)lithiation.

The Role of Charge-Lattice Coupling

While up until now we have primarily discussed the crystallographic aspects of lithium insertion, one cannot ignore the fact that electrons must also be injected into and diffuse through the material in parallel to the ions.[68,69] While oxides like $LiCoO_2$ are well-known to undergo insulator-to-metal transitions that facilitate this process,[70] polyanionic hosts are far more insulating and require careful carbon-coating to cycle well.[6,71] This is because the localization of an electron during charge transport can trigger a prominent structural distortion. This is referred to as a small polaron as long as the length scale of the distortion is comparable to that of the primitive unit cell of the host structure.[72,73]

In any discussion of electrical conductivity, vanadium oxides are usually the best place to begin. V_2O_5, which has been studied almost continuously for over forty years, was first proposed as a Li-ion intercalation host,[75] due to the abundance of interlayer sites capable of accommodating lithium ions, readily accessible $V^{5+/4+}$ and $V^{4+/3+}$ redox couples, and strong enthalpic driving forces for lithiation.[75–77] Recently, Banerjee and co-workers used scanning transmission X-ray microscopy (STXM) to study the correlation between charge localization inhomogeneities and structural distortions induced by lithiation of V_2O_5 nanowires shown in Figure 5.[74,78] Using X-ray absorption near-edge structure and hard-energy X-ray photoemission spectro-

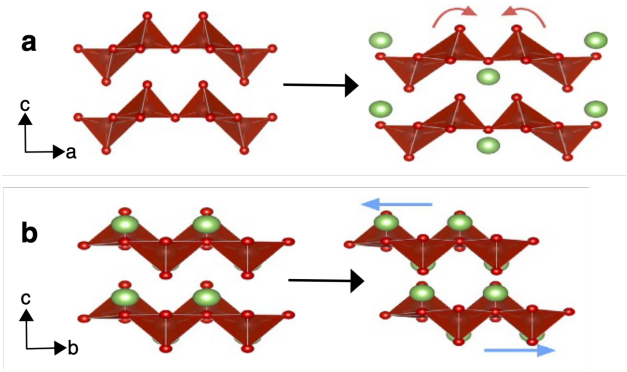

Figure 5: As the V_2O_5 layered structure is lithiated, it undergoes a series of phase transformations, first to the puckered η-phase shown in (a); upon further lithiation, an in-plane shift transforms the η-phase to the δ-phase shown in (b).[74]

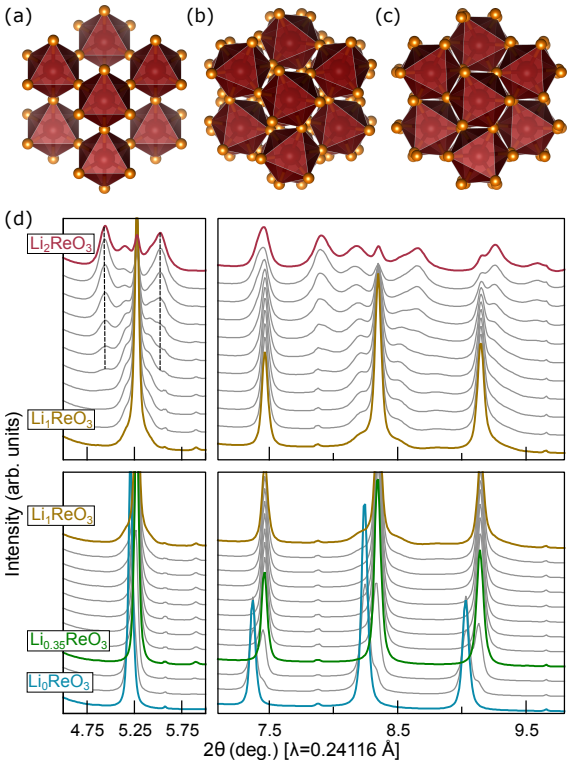

Figure 6: Illustration of the structural distortion that results in a twisting of the close-packed planes of oxygen in (a) ReO_3, (b) $LiReO_3$, and (c) Li_2ReO_3. (d) *Operando* synchrotron X-ray diffraction patterns of ReO_3 throughout a complete discharge to Li_2ReO_3.[79]

scopies to support the theoretical predictions of a distinctive polaronic state, they showed that the polaron hopping barrier in V_2O_5 both impedes electron diffusion and results in lithiation gradients across individual nanowires.

Additionally, a combination of spectral assignments and DFT calculations suggested that lithiating V_2O_5 produces localized reduction of specific vanadium sites via the electron residing in the neighboring V $3d_{xy}$ orbitals, the lowest-lying states in the conduction band. Therefore, small polaron formation seems to be the origin of slow lithium ion diffusion in V_2O_5, and the accelerated kinetics seen when nanostructured can be attributed to overcoming slow small polaron hopping rather than shortening of the diffusion path lengths.

Not long after the work of Banerjee and co-workers,[74] some of us began to study the metallic oxide ReO_3 to determine if this type of polaronic charge transport was truly the origin of the rotational distortions seen in polyanionic phases.[79] The defect perovskite structure is comprised of a perfectly cubic network of corner-sharing octahedra, where the vacancy on the *A*-site creates a three-dimensional network of interstitials that Murphy and co-workers demonstrated can accommodate up to two lithium ions per formula unit when treated with *n*-BuLi.[80] This combination of intrinsic metallic conductivity and pathways for ion diffusion offered an ideal system for exploring the correlations between ionic and electronic transport during lithium

ion insertion.

Operando synchrotron XRD experiments showed that on discharge, a solid solution of Li_xReO_3 forms as small amounts of lithium are inserted, but as the lithium content approaches $x = 1$, there is a distortion to a hexagonal phase.[80,81] This transformation is driven by correlated rotation of the octahedra along the [111] direction in tandem with a contraction along the *c*-axis in order to better coordinate the small lithium ions within the rather large *A*-site interstitial (see Figure 6 and Supporting Information). Interestingly, while strictly speaking ReO_3 is a close-packed oxide, the substantial covalency within the ReO_6 octahedra makes them very rigid, more akin to the main group polyhedra in polyanionic hosts. This is very apparent from the fact that the intra-octahedral O–Re–O angles are maintained at 90° whereas the inter-polyhedral angles bend from 180° to 145° in Li_xReO_3 and ultimately to 138° in the end member Li_2ReO_3. These distortions significantly limit the long-term cycling stability, which is unsurprising given that large changes to the unit cell volume are known to detrimentally effect electrodes, driving particle cracking and de-wetting from the current collector.[82–84] These observations seem to suggest that, despite clear evidence that polarons play a role in V_2O_5, the metallic character of ReO_3 implies the structural distortions during cycling are more likely driven by local strains rather than charge hopping through the lattice.

Case Studies

Layered Rock Salts

The conventional oxide cathode, the *layered rock salt* $LiCoO_2$, is composed of slabs of edge-sharing CoO_6 octahedra separated by layers of positively charged lithium ions that screen the electrostatic repulsion between anions. As lithium is removed from the parent structure, the electrostatic repulsion between the neighboring layers of CoO_6 results in an elongation along the *c*-axis (stacking direction) of the unit cell.[85] This expansion continues to the point that when all the lithium is removed (i.e., CoO_2) the layers *slip* to the CdI_2-type structure (Figure 7).[86] Unlike the $LiCoO_2$ structure, this polymorph is unlikely to undergo lithium insertion since the now vacant lithium site shares parallel faces with the CoO_6 octahedra—this coordination environment is energetically disfavored due to the strong Coulombic repulsion between lithium and cobalt at these small distances.

Alternatively, in the layered transition-metal disulfides (TMDs; $Li_{1-x}MS_2$, M = Ti, V), both the lithiated and delithiated phases adopt the CdI_2 structure type. The larger anion size and increased polarizability of sulfur more effectively screens the lithium–transition-metal repulsion through the shared octahedral faces such that the layer slip is not necessary.

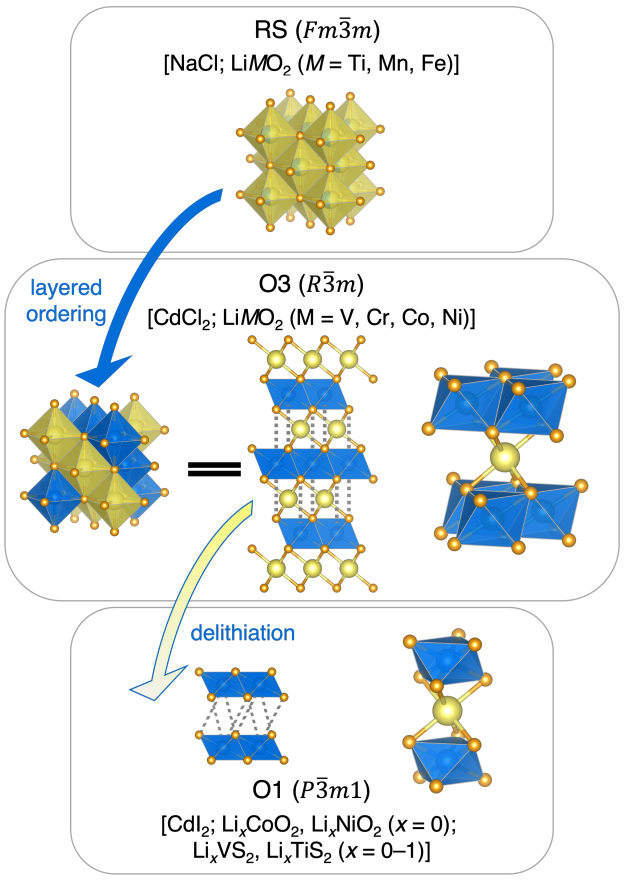

Figure 7: Schematic relating disordered rock salt (RS, top), layered rock salt oxides (O3, middle), and delithiated layered rock salt oxides (O1, bottom), with several composition examples given. The different connectivity of the lithium site is highlighted, where it shares edges with the top and bottom MO_6 layers in the O3 phase while sharing faces in the O1 phase.

Significant effort has been invested in understanding how the transition metal identity influences the layer stacking, particularly in regard to how the stacking changes and how the transition metals migrate during electrochemical cycling. We point the reader to recent reviews by Delmas *et al.*,[87] Clément *et al.*,[88] and Manthiram,[89] which address these points and show how different sections of the community have reached different interpretations. Briefly, cobalt has the longest history and has been used most frequently in portable devices; however, its cost is prohibitive for large scale use, particular with the projected increase in demand for energy storage systems. Nickel is attractive due to the diminished geopolitical issues and high cell potential, but taken alone (e.g., $LiNiO_2$) there are thermal stability concerns. Manganese in isolation (e.g., $LiMnO_2$) is not stable in the layered rock salt structure, but is an advantageous choice when paired with other transition metals (particularly with reference to stabilizing nickel) and for being abundant, low cost, and the least environmentally harmful. Finally, aluminum incorporation decreases the capacity as it replaces some of the redox active transition metals, but its inclusion is rationalized via the improved stability, which

is often explained as inhibiting transition metal migration or dissolution via electronic effects. Combining these factors, one can understand why $LiNi_{1/3}Co_{1/3}Mn_{1/3}O_2$ (NMC, or more specifically NMC333) and $LiNi_{0.70}Co_{0.15}Al_{0.15}O_2$ (NCA) are compositions frequently encountered in the modern literature and in commercialized technologies.

Transition-Metal Silicates

Lithium-containing, transition-metal silicates provide a rich structural and compositional space to begin examining how the flexibility and connectivity of a structure can influence its cycling performance. Much of the early research in this structure type focused on iron orthosilicate and its low- and high-temperature polymorphs. First reported by Thomas and co-workers, Li_2FeSiO_4 exhibits three polymorphs that are all permutations of corner-sharing tetrahedrally coordinated Fe, Si, and Li.[24]

The topology shifts from all corner-sharing in the low-temperature phase, LFS@200 ($Pmn2_1$, #31), to one shared edge in LFS@700 ($P2_1/n$, #14), and two shared edges in the high-temperature polymorph LFS@900 ($Pmnb$, #62) as seen in Figure 8. Sirisopanaporn and co-workers showed that this change in connectivity decreases the average Fe–O distance due to denser packing that results from the introduction of shared edges with the smaller LiO_4 tetrahedra.[90] They concluded that these shorter Fe–O distances, which imply a stronger degree of covalency, should directly impact the position of the $Fe^{3+/2+}$ couple. Galvanostatic and potentiostatic intermittent titration techniques confirmed that the $Fe^{3+/2+}$ potential moves from 3.10 V to 3.00 V to 2.90 V as the Fe–O length contracts from 2.076 to 2.026 Å, moving from the low-temperature

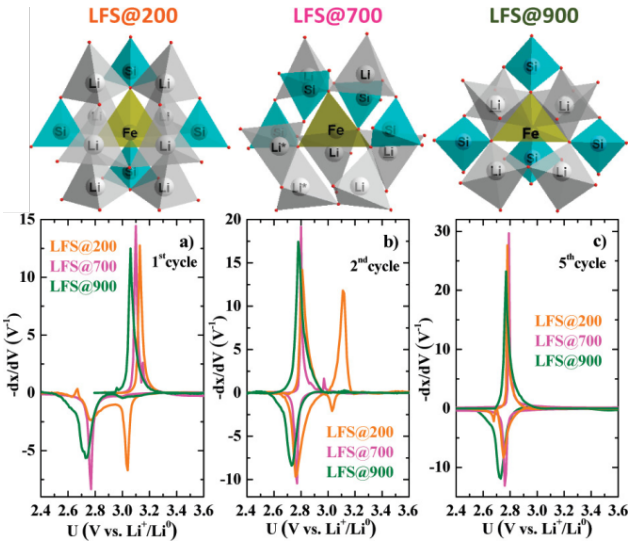

Figure 8: Derivative plots of PITT measurements showing (a) the separation in the location of the $Fe^{3+/2+}$ redox couple based on polymorph on the first cycle followed by subsequent merging of features at 2.8 V by the 5th cycle in (c).[90]

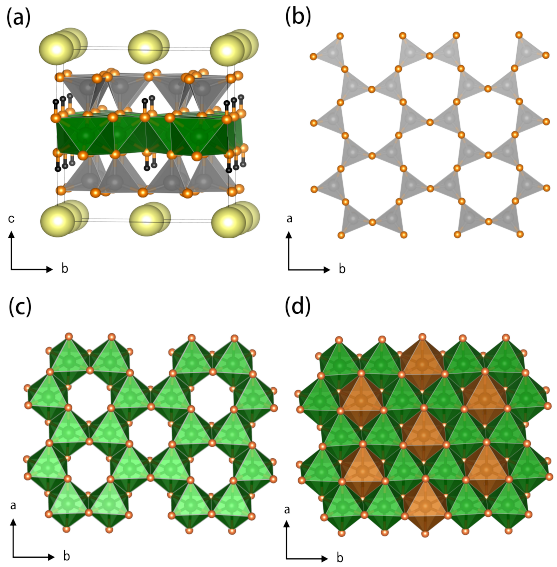

Figure 9: (a) Structure of a typical 2:1 phyllosilicate containing layers of corner-sharing SiO_4 tetrahedra (gray, b) sandwiching a layer of edge-sharing FeO_6 octahedra. Potassium ions (yellow) sit in the interlayer space to balance the negatively charged slabs. There are two metal sites present in the octahedral layer, a "honeycomb" site and an interstitial site depicted in green and brown in (c) and (d).[91]

to high-temperature polymorph. However, the authors noticed significant air and moisture sensitivity, in addition to a re-ordering of the metals upon extended cycling inferred from a shift in the operating potential, as seen in Figure 8.

Building on these reports, our group first investigated $LiFeSi_2O_6$, a member of the pyroxene family, which consists of edge-sharing chains of FeO_6 octahedra that are linked through corner-sharing chains of SiO_4 tetrahedra, with lithium sitting between the chains. Unlike the highly reversible orthosilicates, this material cycled against lithium at C/50 resulted in a faradaic process centered around 2 V versus Li/Li^+ providing a capacity of around 48 mAh/g, or roughly 40% of theoretical capacity. We concluded the low overall capacity was due to poor kinetics of ionic diffusion after cells cycled at C/200 were able to cycle at 60% of theoretical capacity and efforts made to increase electrical conductivity via carbon coating resulted in minimal gains.

To overcome the rigid nature of the silicate tetrahedra, the phyllosilicate family—which consists of a more open framework of well-segregated layers of transition metals and silicate groups akin to $LiCoO_2$—offers an interesting contrast. The structure of a typical 2:1 phyllosilicate, like muscovite $KFe_{2.75}Si_{3.25}O_{10}(OH)_2$, is composed of a layer of edge-sharing transition-metal octahedra wedged between two layers of corner-sharing SiO_4 tetrahedra that make up the polyanionic framework. Surprisingly, the cycling data reported by Zhou *et al.* showed that while a reversible faradaic feature centered around 2.5 V could be obtained, a maximum of 40% of the theoretical capacity, could be obtained.[91] A *b*-value analysis, which can help distinguish surface

capacitance from bulk intercalation, showed two distinct linear regions of slope 0.83 and 0.62 when moving from low to high sweep rate, respectively. These values lie between the expected 0.5 for a purely intercalation based process and 1.0 for surface-controlled electrochemistry, indicating there is a mix of contributions to the overall capacity.

The presence of surface-dominated electrochemical processes suggests that lithium cannot access the interlayer spacing occupied by potassium, which is consistent with work that shows K-based clays are particularly difficult to ion exchange when compared to the analogous Li- and Na-based clays. As a result, it was concluded that the inability to displace the interlayer potassium is what causes the electrochemistry to be isolated to the surface and limits the material's accessible capacity.[91] This observation highlights the importance of thinking beyond simply the structural topology and that there is a need to carefully consider the nature of the bonding for all species within the structure in order to better understand the electrochemical performance.

In order to access more of the theoretical capacity in these materials, Stiles *et al.* examined the ferripyrophyllite, $Fe_2Si_4O_{10}(OH)_2$, a direct analogue to muscovite that does not contain potassium ions in the interlayer space.[92] In contrast to muscovite, the cycling of this material versus lithium resulted in a reversible capacity near 80 mAh/g, corresponding to roughly 1.25 units of Li per formula unit as opposed to 64 mAh/g for a single Li. Obtaining over one Li per formula unit suggests that the mechanism of lithiation involves both the interstitial sites in the transition-metal layer, as observed in muscovite, and the interlayer space.

$LiFePO_4$

In stark contrast to the silicates, $LiFePO_4$ (LFP) is an example of a polyanionic electrode that exhibits exceptionally fast rate performance despite experiencing fairly significant structural deformation during cycling.[93] $LiFePO_4$, which can be found in nature as the mineral triphyllite, was first reported by Goodenough and co-workers in 1997 when they showed that lithium could be extracted reversibly from the ordered olivine structure.[94,95] Early work on this phase identified substantial challenges associated with lithium ion diffusion due to the one-dimensional channels parallel to the *b*-axis that lithium ion conduction occurs through,[96] which was ultimately found to be caused by the presence of antisite defects that mix the lithium and iron in the site that obstruct and prevent efficient charge transport.[97,98]

The facile chemical extraction of lithium from LFP results in the isostructural iron phosphate ($FePO_4$), which other than the absence of lithium, differs by the cooperative rotation of the polyhedral network (see Supporting Information). Since these rotations are parallel to the 1D lithium diffusion pathways, they do not interrupt lithium movement through the structure and result in rapid ionic diffusion. While

exhibiting slightly lower energy density and voltage than the rock salt phases, the improved safety and more sustainable composition (due to the absence of cobalt) has made it an attractive alternative for high cycle-life applications.

Wadsley–Roth Shear Phases

As discussed, the insertion and removal of lithium from perovskitic ReO_3 induces highly correlated rotations of the Re polyhedra, ultimately leading to large polarizations and rapid capacity fade. Even in the early 1980's Cava, Murphy, and Zahurak recognized the detrimental impact these kinds of transformations could have on the ability to move ions through the lattice. In fact, they explicitly note that crystallographic shear introduces edge-sharing into the corner-shared ReO_3 framework and stabilizes the host structures against severe distortion on lithium insertion; thus enhancing kinetics and reducing hysteresis.[99] To overcome this barrier, they suggested that the introduction of shear planes would effectively pin these octahedral rotations at edge-shared boundaries within the structure and impart greater structural stability during cycling. In this section, we will examine the impact that suppression of the structural deformations has on the performance of several materials. Following this logic, the Wadsley–Roth phases have attracted an increasing amount of attention.[100–103]

Wadsley–Roth phases are derived from the ReO_3 structure by introducing crystallographic shear through the removal of a plane of oxide ions to yield alternating layers of edge-sharing and corner-sharing octahedral

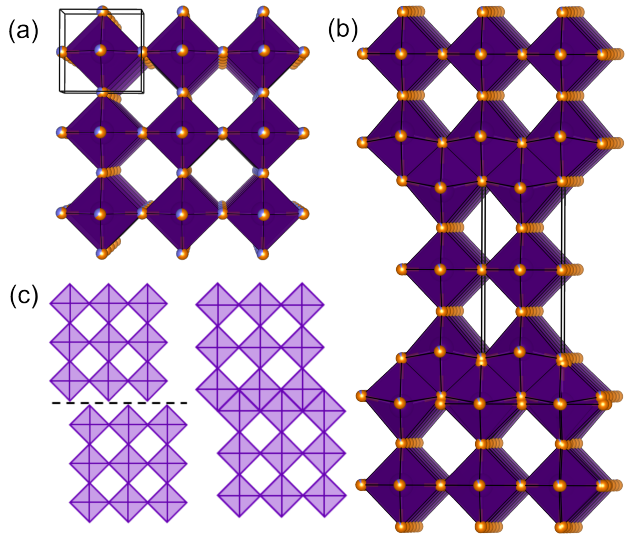

Figure 10: (a) The defect perovskite structure of NbO_2F with corner-sharing octahedra. (b) The related shear structure, Nb_3O_7F, with layers of edge-sharing and corner-sharing octahedra formed by the removal of an anionic plane of atoms from the NbO_2F structure. (c) Representative diagram of the shear relationship between NbO_2F and Nb_3O_7F.[104]

units (Figure 10, 11),[105–112] and have been extensively reviewed by Anderson.[113] In particular, Nb-based compositions like Nb_3O_7F, which is a shear-derivative of the perovskite NbO_2F,[114] offer particularly interesting insights. Nb_3O_7F crystallizes in a less common one-dimensional shear structure, with the planes running along a single crystallographic axis rather than the two-dimensional blocks that are more common in shear structures (Figure 10c).[115] Previous studies had demonstrated that both NbO_2F and Nb_3O_7F show reversible lithiation,[116–119] but more recently Bashian *et al.* investigated the structural relationship between the two phases (Figure 10).[104] They found that while lithiation of the perovskitic NbO_2F occurred through similar twisting of the octahedra, the shear planes in Nb_3O_7F suppressed those rotations and helped to increase the structural stability during cycling.

Yet, because of the one-dimensional nature of the shear, delithiation of Nb_3O_7F introduced significant disorder in the stacking of the planes, disrupting the lithium ion diffusion channels in the structure and resulting in poor capacity retention over multiple cycles. This seems to suggest that while Nb_3O_7F was indeed

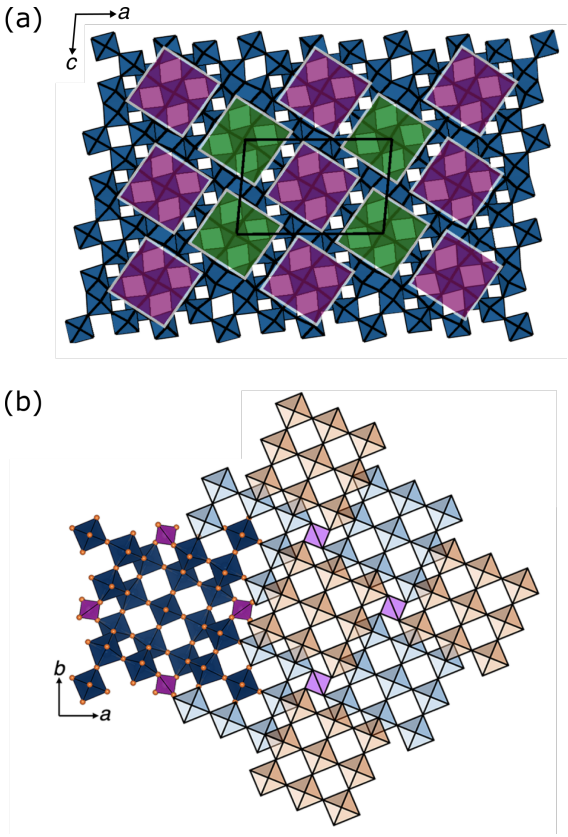

Figure 11: (a) The Wadsley–Roth shear structure $TiNb_2O_7$, where the $(3 \times 3)_\infty$ blocks of ReO_3-like octahedra are shaded purple and green, and are offset by $1/2b$ in the structure.[120] (b) The Wadsley–Roth shear structure PNb_9O_{25}, where the left-hand side depicts the real structure, and on the right, a scheme showing the $3 \times 3 \times 1$ blocks of Nb–O octahedra offset to create corner- and edge-sharing moieties. Half-occupancy tetrahedral sites, filled by P, bridge the offset Nb–O blocks. The tan and blue colored octahedral blocks on the right side indicate their relative positions in the c-direction.[121]

stabilized by the presence of the crystallographic shear, the one-dimensional nature still left it susceptible to the deformation and indicated multiple shear planes in orthogonal directions are needed to fully stabilize these structures.

A slightly more complex example of a Wadsley–Roth phase can be found in $M\mathrm{Nb_9O_{25}}$ (M = V or P), where the structure contains 3 × 3 blocks of $\mathrm{NbO_6}$ octahedra that produce a half-occupied tetrahedral M-site bridging the blocks (Figure 11b).[122,123] The electrochemical properties of these phases were first characterized by Masquelier and co-workers, and more recently revisited by Preefer *et al.*,[121] who demonstrated that the nature of the element occupying the tetrahedral site can significantly impact the material's electrochemical performance.[124] Interestingly, they found that replacing redox-inactive phosphorous with vanadium significantly decreased the rate performance and capacity retention due to an irreversible reduction of the vanadium. So while crystallographic shear can certainly limit the detrimental structural distortions upon (de)lithiation, the composition of the reinforcing subunits must also be carefully considered.

As a final example, we consider $\mathrm{TiNb_2O_7}$, which is an example of a shear phase that shows extremely robust cycling due to the more efficient suppression of these phase transformations during cycling.[120,125] This phase, illustrated in Figure 11a, is made up of blocks of corner-connected Ti/Nb–O octahedra where the blocks are three octahedra wide and three octahedra long, and are infinitely connected in each plane with crystallographic shear planes at the borders of these $\mathrm{ReO_3}$-type regions.[126] This motif, denoted $(3\times3)_\infty$, creates multiple orthogonal crystallographic shear planes that drastically limit structural distortions upon (de)lithiation. Since this phase has already been extensively reviewed by Griffith and many other titans in the field,[127] we will simply conclude by remarking that it can accommodate a whopping five lithium per formula unit to provide a maximum theoretical capacity of 388 mAh/g. This large capacity that can be obtained at fairly high rates makes it extremely competitive, even against graphitic anodes, and has ultimately led to efforts to commercialize it by Toshiba.[127] Therefore, this should serve as an important example of how careful consideration of structural factors, while paying close attention to the sustainability of the composition, can lead to exceptionally promising future technologies.

Summary and Outlook

Before concluding, it would be prudent to add the caveat that most of the materials we have discussed are oxide-based phases, which strike a delicate balance between ionic and covalent bonding, and the observed trends may not readily translate to other anionic compositions. As Zeier and co-workers highlighted in their discussion of sulfide-based lithium ion conductors, the structural requirements are quite different when the lattice becomes significantly more polarizable.[128] Softer lattices do not need to distort to the same extent

that the rigid oxoanionic groups discussed in this article do to sufficiently solvate the diffusing species.

In this perspective, we have tried to demonstrate the complex (and frequently competing) material requirements that all must work in perfect harmony to create high performance batteries. Taking all this into consideration, its actually quite amazing that some of the first materials investigated as intercalation electrodes have worked as effectively as they do. The highly correlated nature of the rotational distortions that occur in polyanionic compounds serves to emphasize the substantial degree of atomic rearrangement that these structures experience during cycling. It is therefore quite impressive that these devices work as efficiently as they do, and it is a credit to the myriad of battery scientists and materials chemists who have helped to overcome these complex challenges.

Nevertheless, a number of open questions regarding the optimal structural topologies and compositions for fast diffusion through intercalation hosts still remain. *When do polaronic effects start to interfere with charge transport? How do we,* a priori, *target structural topologies that will deform without interfering with ionic transport? Can we create analogues to the Wadsley–Roth phases that contain higher voltage transition metals like Ni, Mn, Fe, or Co to eventually realize a zero-strain full cell?* All these questions foretell an exciting future for Li-ion electrode materials, which, if answered, could drastically improve the cycle life and rate performance of rechargeable batteries.

Author Information

Corresponding Author

Brent C. Melot – Department of Chemistry and Department of Chemical Engineering and Materials Science, University of Southern California, Los Angeles, California 90089, USA. Email: melot@usc.edu ORCID: 0000-0002-7078-8206

Authors

Jessica L. Andrews – Department of Chemistry, University of Southern California, Los Angeles, California 90089, USA. ORCID: 0000-0001-9794-8903

Michael J. Brady – Department of Chemistry, University of Southern California, Los Angeles, California 90089, USA. ORCID: 0000-0001-9656-0472

Eric T. McClure – Department of Chemistry, University of Southern California, Los Angeles, California 90089, USA. ORCID: 0000-0003-1432-0016

Author Contributions

J.L.A., M.J.B., and E.T.M. are listed in alphabetical order, and have contributed to this work equally. The manuscript was written through contributions of all authors. All authors have given approval to the final version of the manuscript.

Biographies

Jessica L. Andrews is a Graduate Student Researcher in the Department of Chemistry at the University of Southern California, under the supervision of Prof. Brent Melot. She is the recipient of a 2021 NSF Graduate Research Fellowship. She received her B.S. in Chemistry from the University of California, Santa Barbara in 2019. Her current research focuses on synthesizing and studying materials that can electrochemically (de)insert fluoride ions at room temperature.

Michael J. Brady is a Graduate Student Researcher in the Department of Chemistry at the University of Southern California, under the supervision of Prof. Brent Melot. He received his B.S. in Chemistry from the University of California, Santa Barbara in 2018. His current research focuses on the synthesis and characterization of both solid electrolytes and cathode materials for lithium and fluoride ion batteries.

Eric T. McClure is a Postdoctoral Researcher in the Department of Chemistry at the University of Southern California, working in the laboratory of Prof. Brent Melot. His current research focuses on the structural impacts of chemical and electrochemical ion insertion. He received his Ph.D. in Chemistry from The Ohio State University in 2019, under the supervision of Prof. Patrick Woodward.

Brent C. Melot is an Associate Professor of Chemistry, Chemical Engineering, and Materials Science at the University of Southern California. He received his Ph.D. from the Materials Department at the University of California, Santa Barbara under the supervision of Ram Seshadri and subsequently joined the Laboratoire de Réactivité et Chimie des Solides in Amiens as a postdoctoral research associate under Jean-Marie Tarascon. Since starting his independent career in 2012, his group has focused on developing a deeper understanding of how the crystal structure and composition of materials influence their functional properties. They are broadly interested in materials for a diverse range of applications including halide perovskite light absorbers, frustrated magnetism in oxides, as well as alkali and fluoride insertion hosts for energy storage.

Acknowledgments

J.L.A. acknowledges support from the National Science Foundation Graduate Research Fellowship Program under Grant No. DGE-1842487. M.J.B., E.T.M., and B.C.M. acknowledge support through a CAREER award from the National Science Foundation under Grant No. DMR-1554204. B.C.M. also gratefully acknowledges the Research Corporation for Science Advancement for a Cottrell Scholar award and multiple Scialog grants that helped formulate many of the ideas discussed.

References

(1) Lazzari, M.; Scrosati, B. A Cyclable Lithium Organic Electrolyte Cell Based on Two Intercalation Electrodes. *J. Electrochem. Soc.* **1980**, *127*, 773.

(2) Thackeray, M. M.; Johnson, P. J.; de Picciotto, L. A.; Bruce, P. G.; Goodenough, J. B. Electrochemical extraction of lithium from $LiMn_2O_4$. *Mater. Res. Bull.* **1984**, *19*, 179–187.

(3) Chebiam, R. V.; Prado, F.; Manthiram, A. Soft Chemistry Synthesis and Characterization of Layered $Li_{1-x}Ni_{1-y}Co_yO_2$ ($0 \leq x \leq 1$ and $0 \leq y \leq 1$). *Chem. Mater.* **2001**, *13*, 2951–2957.

(4) Chebiam, R. V.; Kannan, A. M.; Prado, F.; Manthiram, A. Comparison of the chemical stability of the high energy density cathodes of lithium-ion batteries. *Electrochem. Commun.* **2001**, *3*, 624–627.

(5) Padhi, A. K.; Nanjundaswamy, K. S.; Goodenough, J. B. Phospho-olivines as Positive-Electrode Materials for Rechargeable Lithium Batteries. *J. Electrochem. Soc.* **1997**, *144*, 1188.

(6) Ravet, N.; Goodenough, J.; Besner, S.; Simoneau, M.; Hovington, P.; Armand, M. Improved iron based cathode material. Proceedings of the 196th ECS meeting, Honolulu, extended abstract. 1999.

(7) Armand, M. B. In *Materials for Advanced Batteries*; Murphy, D. W., Broadhead, J., Steele, B. C. H., Eds.; NATO Conference Series; Springer US: Boston, MA, 1980; pp 145–161.

(8) Armand, M. B. In *Fast Ion Transport in Solids: Solid State Batteries and Devices*; Van Gool, W., Ed.; North Holland Publishers, 1973; pp 665–673.

(9) Dahn, J. R.; Zheng, T.; Liu, Y.; Xue, J. S. Mechanisms for Lithium Insertion in Carbonaceous Materials. *Science* **1995**, *270*, 590–593.

(10) Poizot, P.; Laruelle, S.; Grugeon, S.; Dupont, L.; Tarascon, J.-M. Nano-sized transition-metal oxides as negative-electrode materials for lithium-ion batteries. *Nature* **2000**, *407*, 496–499.

(11) Murphy, D. W.; Christian, P. A.; DiSalvo, F. J.; Carides, J. N. Vanadium Oxide Cathode Materials for Secondary Lithium Cells. *J. Electrochem. Soc.* **1979**, *126*, 497.

(12) Murphy, D. W.; Christian, P. A. Solid State Electrodes for High Energy Batteries. *Science* **1979**, *205*, 651–656.

(13) Steele, B. In *Fast Ion Transport in Solids: Solid State Batteries and Devices*; Van Gool, W., Ed.; North Holland Publishers, 1973; pp 103–109.

(14) Mizushima, K.; Jones, P. C.; Wiseman, P. J.; Goodenough, J. B. Li_xCoO_2 ($0< x <1$): A new cathode material for batteries of high energy density. *Mater. Res. Bull.* **1980**, *15*, 783–789.

(15) Tarascon, J.-M.; Armand, M. Issues and challenges facing rechargeable lithium batteries. *Nature* **2001**, *414*, 359–367.

(16) Melot, B. C.; Scanlon, D. O.; Reynaud, M.; Rousse, G.; Chotard, J.-N.; Henry, M.; Tarascon, J.-M. Chemical and Structural Indicators for Large Redox Potentials in Fe-Based Positive Electrode Materials. *ACS Appl. Mater. Interfaces* **2014**, *6*, 10832–10839.

(17) Yabuuchi, N.; Ohzuku, T. Novel lithium insertion material of $LiCo_{1/3}Ni_{1/3}Mn_{1/3}O_2$ for advanced lithium-ion batteries. *J. Power Sources* **2003**, *119–121*, 171–174.

(18) Guilmard, M.; Pouillerie, C.; Croguennec, L.; Delmas, C. Structural and electrochemical properties of $LiNi_{0.70}Co_{0.15}Al_{0.15}O_2$. *Solid State Ion.* **2003**, *160*, 39–50.

(19) Thackeray, M. M.; David, W. I. F.; Bruce, P. G.; Goodenough, J. B. Lithium insertion into manganese spinels. *Mater. Res. Bull.* **1983**, *18*, 461–472.

(20) Wiers, B. M.; Foo, M.-L.; Balsara, N. P.; Long, J. R. A Solid Lithium Electrolyte via Addition of Lithium Isopropoxide to a Metal–Organic Framework with Open Metal Sites. *J. Am. Chem. Soc.* **2011**, *133*, 14522–14525.

(21) Park, S. S.; Tulchinsky, Y.; Dincâ, M. Single-Ion Li^+, Na^+, and Mg^{2+} Solid Electrolytes Supported by a Mesoporous Anionic Cu–Azolate Metal–Organic Framework. *J. Am. Chem. Soc.* **2017**, *139*, 13260–13263.

(22) Cepeda, J.; Pérez-Yáñez, S.; Beobide, G.; Castillo, O.; Goikolea, E.; Aguesse, F.; Garrido, L.; Luque, A.; Wright, P. A. Scandium/Alkaline Metal–Organic Frameworks: Adsorptive Properties and Ionic Conductivity. *Chem. Mater.* **2016**, *28*, 2519–2528.

(23) Masquelier, C.; Croguennec, L. Polyanionic (Phosphates, Silicates, Sulfates) Frameworks as Electrode Materials for Rechargeable Li (or Na) Batteries. *Chem. Rev.* **2013**, *113*, 6552–6591.

(24) Nytén, A.; Abouimrane, A.; Armand, M.; Gustafsson, T.; Thomas, J. O. Electrochemical performance of Li_2FeSiO_4 as a new Li-battery cathode material. *Electrochem. Commun.* **2005**, *7*, 156–160.

(25) Zhou, F.; Cococcioni, M.; Kang, K.; Ceder, G. The Li intercalation potential of $LiMPO_4$ and $LiMSiO_4$ olivines with M=Fe, Mn, Co, Ni. *Electrochem. Commun.* **2004**, *6*, 1144–1148.

(26) Rousse, G.; Tarascon, J. M. Sulfate-Based Polyanionic Compounds for Li-Ion Batteries: Synthesis, Crystal Chemistry, and Electrochemistry Aspects. *Chem. Mater.* **2014**, *26*, 394–406.

(27) Park, M.; Zhang, X.; Chung, M.; Less, G. B.; Sastry, A. M. A review of conduction phenomena in Li-ion batteries. *J. Power Sources* **2010**, *195*, 7904–7929.

(28) Iton, Z. W. B.; See, K. A. Multivalent Ion Conduction in Inorganic Solids. *Chem. Mater.* **2022**, *34*, 881–898.

(29) Kalinin, S.; Balke, N.; Jesse, S.; Tselev, A.; Kumar, A.; Arruda, T. M.; Guo, S.; Proksch, R. Li-ion dynamics and reactivity on the nanoscale. *Mater. Today* **2011**, *14*, 548–558.

(30) Green, P. F. *Kinetics, Transport, and Structure in Hard and Soft Materials*; CRC Press, 2005.

(31) Mehrer, H., Ed. *Diffusion in Solid Metals and Alloys*; Springer, 1990.

(32) Bruce, P. G. Solid-state chemistry of lithium power sources. *Chem. Commun.* **1997**, *1*, 1817–1824.

(33) Melot, B. C.; Rousse, G.; Chotard, J.-N.; Ati, M.; Rodríguez-Carvajal, J.; Kemei, M. C.; Tarascon, J.-M. Magnetic Structure and Properties of the Li-Ion Battery Materials $FeSO_4F$ and $LiFeSO_4F$. *Chem. Mater.* **2011**, *23*, 2922–2930.

(34) Barpanda, P.; Ati, M.; Melot, B. C.; Rousse, G.; Chotard, J.-N.; Doublet, M.-L.; Sougrati, M. T.; Corr, S. A.; Jumas, J. C.; Tarascon, J.-M. A 3.90 V Fe-based fluorosulphate material for Li-ion batteries crystallizing in the *triplite* structure. *Nat. Mater.* **2011**, *10*, 772–779.

(35) Ati, M.; Melot, B. C.; Rousse, G.; Chotard, J.-N.; Barpanda, P.; Tarascon, J.-M. Structural and Electrochemical Diversity in $LiFe_{1-\delta}Zn_{\delta}SO_4F$ Solid Solution: A Fe-Based Positive-Electrode Material. *Angew. Chem. Int. Ed.* **2011**, *50*, 10574–10577.

(36) Neilson, J. R.; McQueen, T. M. Bonding, Ion Mobility, and Rate-Limiting Steps in Deintercalation Reactions with $ThCr_2Si_2$-type KNi_2Se_2. *J. Am. Chem. Soc.* **2012**, *134*, 7750–7757.

(37) Howard, C. J.; Stokes, H. T. Group-Theoretical Analysis of Octahedral Tilting in Perovskites. *Acta Cryst.* **1998**, *B54*, 782–789.

(38) Howard, C. J.; Kennedy, B. J.; Woodward, P. M. Ordered double perovskites – a group-theoretical analysis. *Acta Cryst.* **2003**, *B59*, 463–471.

(39) Howard, C. J.; Stokes, H. T. Octahedral tilting in cation-ordered perovskites – a group-theoretical analysis. *Acta Cryst.* **2004**, *B60*, 674–684.

(40) Howard, C. J.; Stokes, H. T. Structures and phase transitions in perovskites – a group-theoretical approach. *Acta Cryst.* **2005**, *A61*, 93–111.

(41) Giddy, A. P.; Dove, M. T.; Pawley, G. S.; Heine, V. The determination of rigid-unit modes as potential soft modes for displacive phase transitions in framework crystal structures. *Acta Cryst.* **1993**, *A49*, 697–703.

(42) Swainson, I.; Chi, L.; Her, J.-H.; Cranswick, L.; Stephens, P.; Winkler, B.; Wilson, D. J.; Milman, V. Orientational ordering, tilting and lone-pair activity in the perovskite methylammonium tin bromide, $CH_3NH_3SnBr_3$. *Acta Cryst.* **2010**, *B66*, 422–429.

(43) Ati, M.; Melot, B. C.; Chotard, J.-N.; Rousse, G.; Reynaud, M.; Tarascon, J.-M. Synthesis and electrochemical properties of pure $LiFeSO_4F$ in the triplite structure. *Electrochem. Commun.* **2011**, *13*, 1280–1283.

(44) Lister, S. E.; Rixom, V. J.; Evans, J. S. O. Structural and Mechanistic Studies of the Dehydration of $MoO_2PO_3OH{\cdot}H_2O$ and the In situ Identification of Two New Molybdenum Phosphates. *Chem. Mater.* **2010**, *22*, 5279–5289.

(45) Yamauchi, K. Theoretical Prediction of Multiferroicity in $SmBaMn_2O_6$. *J. Phys. Soc. Jpn.* **2013**, *82*, 043702.

(46) Müller, M.; Dinnebier, R. E.; Dippel, A.-C.; Stokes, H. T.; Campbell, B. J. A symmetry-mode description of rigid-body rotations in crystalline solids: a case study of $Mg(H_2O)_6RbBr_3$. *J. Appl. Crystallogr.* **2014**, *47*, 532–538.

(47) McClure, E. T.; Hodgkins, T. L.; Djurovich, P. I.; Thompson, M. E.; Melot, B. C. Influence of Dimethyl Sulfoxide on the Structural Topology during Crystallization of PbI_2. *Inorg. Chem.* **2020**, *59*, 16799–16803.

(48) Campbell, B. J.; Evans, J. S. O.; Perselli, F.; Stokes, H. T. Rietveld refinement of structural distortion-mode amplitudes. *IUCr Comput. Comm. Newsl.* **2007**, *8*, 81–95.

(49) Orobengoa, D.; Capillas, C.; Aroyo, M. I.; Perez-Mato, J. M. *AMPLIMODES*: symmetry-mode analysis on the Bilbao Crystallographic Server. *J. Appl. Crystallogr.* **2009**, *42*, 820–833.

(50) Perez-Mato, J. M.; Orobengoa, D.; Aroyo, M. I. Mode crystallography of distorted structures. *Acta Cryst.* **2010**, *A66*, 558–590.

(51) Aroyo, M. I.; Kirov, A.; Capillas, C.; Perez-Mato, J. M.; Wondratschek, H. Bilbao Crystallographic Server II: Representations of crystallographic point groups and space groups. *Acta Cryst.* **2006**, *A62*, 115–128.

(52) Aroyo, M. I.; Perez-Mato, J. M.; Capillas, C.; Kroumova, E.; Ivantchev, S.; Madariaga, G.; Kirov, A.; Wondratschek, H. Bilbao Crystallographic Server: I. Databases and crystallographic computing programs. *Zeitschrift für Krist. - Cryst. Mater.* **2006**, *221*, 15–20.

(53) Stokes, H. T.; Hatch, D. M.; Campbell, B. J. ISOTROPY Software Suite. `iso.byu.edu`.

(54) Campbell, B. J.; Stokes, H. T.; Tanner, D. E.; Hatch, D. M. ISODISPLACE: a web-based tool for exploring structural distortions. *J. Appl. Crystallogr.* **2006**, *39*, 607–614.

(55) Stokes, H. T.; Hatch, D. M. Procedure for obtaining microscopic mechanisms of reconstructive phase transitions in crystalline solids. *Phys. Rev. B* **2002**, *65*, 144114.

(56) Zhou, S.; Barim, G.; Morgan, B. J.; Melot, B. C.; Brutchey, R. L. Influence of Rotational Distortions on Li^+- and Na^+-Intercalation in Anti-NASICON $Fe_2(MoO_4)_3$. *Chem. Mater.* **2016**, *28*, 4492–4500.

(57) Yue, J.-L.; Zhou, Y.-N.; Shi, S.-Q.; Shadike, Z.; Huang, X.-Q.; Luo, J.; Yang, Z.-Z.; Li, H.; Gu, L.; Yang, X.-Q.; Fu, Z.-W. Discrete Li-occupation versus pseudo-continuous Na-occupation and their relationship with structural change behaviors in Fe2(MoO4)3. *Sci. Rep.* **2015**, *5*, 8810.

(58) Bruce, P. G., Ed. *Solid State Electrochemistry*; Cambridge University Press, 1995; p 344.

(59) Van der Ven, A.; Marianetti, C.; Morgan, D.; Ceder, G. Phase transformations and volume changes in spinel LixMn2O4. *Solid State Ion.* **2000**, *135*, 21–32.

(60) Omenya, F.; Chernova, N. A.; Wang, Q.; Zhang, R.; Whittingham, M. S. The Structural and Electrochemical Impact of Li and Fe Site Substitution in LiFePO4. *Chem. Mater.* **2013**, *25*, 2691–2699.

(61) Yu, Y.-S. et al. Dependence on Crystal Size of the Nanoscale Chemical Phase Distribution and Fracture in LixFePO4. *Nano Lett.* **2015**, *15*, 4282–4288.

(62) Abdellahi, A.; Akyildiz, O.; Malik, R.; Thornton, K.; Ceder, G. The thermodynamic stability of intermediate solid solutions in LiFePO4 nanoparticles. *J. Mater. Chem. A* **2016**, *4*, 5436–5447.

(63) Barim, G.; Cottingham, P.; Zhou, S.; Melot, B. C.; Brutchey, R. L. Investigating the Mechanism of Reversible Lithium Insertion into Anti-NASICON $Fe_2(WO_4)_3$. *ACS Appl. Mater. Interfaces* **2017**, *9*, 10813–10819.

(64) Harrison, W.; Chowdhry, U.; Machiels, C.; Sleight, A.; Cheetham, A. Preparation of ferric tungstate and its catalytic behavior toward methanol. *J. Solid State Chem.* **1985**, *60*, 101–106.

(65) Manthiram, A.; Goodenough, J. B. Lithium insertion into $Fe_2(MO_4)_3$ frameworks: Comparison of M = W with M = Mo. *J. Solid State Chem.* **1987**, *71*, 349–360.

(66) Bashian, N. H.; Abdel-Latif, S.; Zuba, M.; Griffith, K. J.; Ganose, A. M.; Stiles, J. W.; Zhou, S.; Scanlon, D. O.; Piper, L. F. J.; Melot, B. C. Transition Metal Migration Can Facilitate Ionic Diffusion in Defect Garnet-Based Intercalation Electrodes. *ACS Energy Lett.* **2020**, *5*, 1448–1455.

(67) Feng, K.; Wang, F.; Zhang, H.; Li, X.; Zhang, H. $Li_3Cr(MoO_4)_3$: a NASICON-type high specific capacity cathode material for lithium ion batteries. *J. Mater. Chem. A* **2018**, *6*, 19107–19112.

(68) Ong, S. P.; Chevrier, V. L.; Ceder, G. Comparison of small polaron migration and phase separation in olivine $LiMnPO_4$ and $LiFePO_4$ using hybrid density functional theory. *Phys. Rev. B* **2011**, *83*, 075112.

(69) Castro, L.; Dedryvère, R.; El Khalifi, M.; Lippens, P.-E.; Bréger, J.; Tessier, C.; Gonbeau, D. The Spin-Polarized Electronic Structure of $LiFePO_4$ and $FePO_4$ Evidenced by in-Lab XPS. *J. Phys. Chem. C* **2010**, *114*, 17995–18000.

(70) Flores, E.; Mozhzhukhina, N.; Aschauer, U.; Berg, E. J. Operando Monitoring the Insulator–Metal Transition of $LiCoO_2$. *ACS Appl. Mater. Interfaces* **2021**, *13*, 22540–22548.

(71) Huang, H.; Yin, S.-C.; Nazar, L. F. Approaching Theoretical Capacity of $LiFePO_4$ at Room Temperature at High Rates. *Electrochem. Solid-State Lett.* **2001**, *4*, A170–A172.

(72) Fröhlich, H. Electrons in lattice fields. *Adv. Phys.* **1954**, *3*, 325–361.

(73) Emin, D. Small Polarons. *Phys. Today* **1982**, *35*, 34.

(74) De Jesus, L. R.; Horrocks, G. A.; Liang, Y.; Parija, A.; Jaye, C.; Wangoh, L.; Wang, J.; Fischer, D. A.; Piper, L. F.; Prendergast, D., et al. Mapping polaronic states and lithiation gradients in individual V_2O_5 nanowires. *Nat. Commun.* **2016**, *7*, 1–9.

(75) Whittingham, M. S. Electrical Energy Storage and Intercalation Chemistry. *Science* **1976**, *192*, 1126–1127.

(76) Chernova, N. A.; Roppolo, M.; Dillon, A. C.; Whittingham, M. S. Layered vanadium and molybdenum oxides: batteries and electrochromics. *J. Mater. Chem.* **2009**, *19*, 2526–2552.

(77) Scanlon, D. O.; Walsh, A.; Morgan, B. J.; Watson, G. W. An ab initio Study of Reduction of V_2O_5 through the Formation of Oxygen Vacancies and Li Intercalation. *J. Phys. Chem. C* **2008**, *112*, 9903–9911.

(78) Handy, J. V.; Luo, Y.; Andrews, J. L.; Bhuvanesh, N.; Banerjee, S. An Atomic View of Cation Diffusion Pathways from Single-Crystal Topochemical Transformations. *Angew. Chem. Int. Ed.* **2020**, *59*, 16385–16392.

(79) Bashian, N. H.; Zhou, S.; Zuba, M.; Ganose, A. M.; Stiles, J. W.; Ee, A.; Ashby, D. S.; Scanlon, D. O.; Piper, L. F. J.; Dunn, B.; Melot, B. C. Correlated Polyhedral Rotations in the Absence of Polarons during Electrochemical Insertion of Lithium in ReO_3. *ACS Energy Lett.* **2018**, *3*, 2513–2519.

(80) Murphy, D. W.; Greenblatt, M.; Cava, R. J.; Zahurak, S. M. Topotactic lithium reactions with ReO_3 related shear structures. *Solid State Ion.* **1981**, *5*, 327–329.

(81) Cava, R.; Santoro, A.; Murphy, D.; Zahurak, S.; Roth, R. The structures of lithium-inserted metal oxides: $LiReO_3$ and Li_2ReO_3. *J. Solid State Chem.* **1982**, *42*, 251–262.

(82) Wang, H.; Jang, Y.-I.; Huang, B.; Sadoway, D. R.; Chiang, Y.-M. TEM Study of Electrochemical Cycling-Induced Damage and Disorder in $LiCoO_2$ Cathodes for Rechargeable Lithium Batteries. *J. Electrochem. Soc.* **1999**, *146*, 473–480.

(83) Dokko, K. In Situ Observation of $LiNiO_2$ Single-Particle Fracture during Li-Ion Extraction and Insertion. *Electrochem. Solid-State Lett.* **1999**, *3*, 125.

(84) Jang, Y.-I.; Huang, B.; Wang, H.; Sadoway, D. R.; Ceder, G.; Chiang, Y.-M.; Liu, H.; Tamura, H. $LiAl_yCo_{1-y}O_2$ ($R\bar{3}m$) Intercalation Cathode for Rechargeable Lithium Batteries. *J. Electrochem. Soc.* **1999**, *146*, 862–868.

(85) Kikkawa, S.; Miyazaki, S.; Koizumi, M. Deintercalated $NaCoO_2$ and $LiCoO_2$. *J. Solid State Chem.* **1986**, *62*, 35–39.

(86) Amatucci, G.; Tarascon, J.-M.; Klein, L. C. CoO_2, The End Member of the Li_xCoO_2 Solid Solution. *J. Electrochem. Soc.* **1996**, *143*, 1114–1123.

(87) Delmas, C.; Carlier, D.; Guignard, M. The Layered Oxides in Lithium and Sodium-Ion Batteries: A Solid-State Chemistry Approach. *Adv. Energy Mater.* **2021**, *11*, 2001201.

(88) Clément, R. J.; Lun, Z.; Ceder, G. Cation-disordered rocksalt transition metal oxides and oxyfluorides for high energy lithium-ion cathodes. *Energy Environ. Sci.* **2020**, *13*, 345–373.

(89) Manthiram, A. A reflection on lithium-ion battery cathode chemistry. *Nat. Commun.* **2020**, *11*, 1550.

(90) Sirisopanaporn, C.; Masquelier, C.; Bruce, P. G.; Armstrong, A. R.; Dominko, R. Dependence of Li_2FeSiO_4 Electrochemistry on Structure. *J. Am. Chem. Soc.* **2011**, *133*, 1263–1265.

(91) Zhou, S.; Howard, E. S.; Liu, J.; Bashian, N. H.; Nolan, K.; Krishnamoorthy, S.; Rangel, G. M.; Sougrati, M.-T.; Prakash, G. K. S.; Page, K.; Melot, B. C. Hydrothermal Preparation, Crystal Chemistry, and Redox Properties of Iron Muscovite Clay. *ACS Appl. Mater. Interfaces* **2017**, *9*, 34024–34032.

(92) Stiles, J. W.; McClure, E. T.; Bashian, N. H.; Tappan, B. T.; Melot, B. C. Reversible Intercalation of Li Ions in an Earth-Abundant Phyllosilicate Clay. *Inorg. Chem.* **2022**,

(93) Kang, B.; Ceder, G. Battery materials for ultrafast charging and discharging. *Nature* **2009**, *458*, 190–193.

(94) Padhi, A. K.; Nanjundaswamy, K. S.; Goodenough, J. B. Phospho-olivines as positive-electrode materials for rechargeable lithium batteries. *J. Electrochem. Soc.* **1997**, *144*, 1188–1194.

(95) Padhi, A. K.; Nanjundaswamy, K. S.; Masquelier, C.; Okada, S.; Goodenough, J. B. Effect of Structure on the Fe^{3+}/Fe^{2+} Redox Couple in Iron Phosphates. *J. Electrochem. Soc.* **1997**, *144*, 1609.

(96) Nishimura, S.-i.; Kobayashi, G.; Ohoyama, K.; Kanno, R.; Yashima, M.; Yamada, A. Experimental visualization of lithium diffusion in Li_xFePO_4. *Nat. Mater.* **2008**, *7*, 707–711.

(97) Liu, H.; Choe, M.-J.; Enrique, R. A.; Orvañanos, B.; Zhou, L.; Liu, T.; Thornton, K.; Grey, C. P. Effects of Antisite Defects on Li Diffusion in $LiFePO_4$ Revealed by Li Isotope Exchange. *J. Phys. Chem. C* **2017**, *121*, 12025–12036.

(98) Malik, R.; Burch, D.; Bazant, M.; Ceder, G. Particle Size Dependence of the Ionic Diffusivity. *Nano Lett.* **2010**, *10*, 4123–4127.

(99) Cava, R. J.; Murphy, D. W.; Zahurak, S. M. Lithium Insertion in Wadsley-Roth Phases Based on Niobium Oxide. *J. Electrochem. Soc.* **1983**, *130*, 2345–2351.

(100) Cheng, Q.; Liang, J.; Zhu, Y.; Si, L.; Guo, C.; Qian, Y. Bulk $Ti_2Nb_{10}O_{29}$ as long-life and high-power Li-ion battery anodes. *J. Mater. Chem. A* **2014**, *2*, 17258–17262.

(101) Griffith, K. J.; Forse, A. C.; Griffin, J. M.; Grey, C. P. High-Rate Intercalation without Nanostructuring in Metastable Nb_2O_5 Bronze Phases. *J. Am. Chem. Soc.* **2016**, *138*, 8888–8899.

(102) Griffith, K. J.; Wiaderek, K. M.; Cibin, G.; Marbella, L. E.; Grey, C. P. Niobium tungsten oxides for high-rate lithium-ion energy storage. *Nature* **2018**, *556*, 556–563.

(103) Deng, Q.; Fu, Y.; Zhu, C.; Yu, Y. Niobium-based oxides toward advanced electrochemical energy storage: recent advances and challenges. *Small* **2019**, *15*, 1804884.

(104) Bashian, N. H.; Preefer, M. B.; Milam-Guerrero, J.; Zak, J. J.; Sendi, C.; Ahsan, S. A.; Vincent, R. C.; Haiges, R.; See, K. A.; Seshadri, R.; Melot, B. C. Understanding the role of crystallographic shear on the electrochemical behavior of niobium oxyfluorides. *J. Mater. Chem. A* **2020**, *8*, 12623–12632.

(105) Wadsley, A. D. Mixed oxides of titanium and niobium. I. *Acta Cryst.* **1961**, *14*, 660–664.

(106) Wadsley, A. D. Mixed oxides of titanium and niobium. II. The crystal structures of the dimorphic forms $Ti_2Nb_{10}O_{29}$. *Acta Cryst.* **1961**, *14*, 664–670.

(107) Roth, R. S.; Wadsley, A. D. Multiple phase formation in the binary system Nb_2O_5–WO_3. I. Preparation and identification of phases. *Acta Cryst.* **1965**, *19*, 26–32.

(108) Roth, R. S.; Wadsley, A. D. Multiple phase formation in the binary system Nb_2O_5–WO_3. II. The structure of the monoclinic phases $WNb_{12}O_{33}$ and $W_5Nb_{16}O_{55}$. *Acta Cryst.* **1965**, *19*, 32–38.

(109) Roth, R. S.; Wadsley, A. D. Multiple phase formation in the binary system Nb_2O_5–WO_3. III. The structures of the tetragonal phases $W_3Nb_{14}O_{44}$ and $W_8Nb_{18}O_{69}$. *Acta Cryst.* **1965**, *19*, 38–42.

(110) Roth, R. S.; Wadsley, A. D. Multiple phase formation in the binary system Nb_2O_5–WO_4. IV. The block principle. *Acta Cryst.* **1965**, *19*, 42–47.

(111) Bursill, L. A.; Hyde, B. G. On the aggregation of Wadsley defects in slightly reduced rutile. *Philos. Mag.* **1971**, *23*, 3–15.

(112) Bursill, L. A.; Hyde, B. G.; Philp, D. K. New crystallographic shear families derived from the rutile structure, and the possibility of continuous ordered solid solution. *Philos. Mag.* **1971**, *23*, 1501–1513.

(113) Anderson, J. In *Intercalation Chemistry*; Whittingham, M. S., Jacobson, A. J., Eds.; 1982; pp 503–538.

(114) Cordier, S.; Roisnel, T.; Poulain, M. Synthesis and characterization of the novel $Nb_3O_5F_5$ niobium oxyfluoride: the term n=3 of the $Nb_nO_{2n-1}F_{n+2}$ series. *J. Solid State Chem.* **2004**, *177*, 3119–3126.

(115) Andersson, S. The description of non-stoichiometric transition metal oxides. A logical extension of inorganic crystallography. *Bulletin de Minéralogie* **1967**, *90*, 522–527.

(116) Bohnke, C.; Bohnke, O.; Fourquet, J. L. Electrochemical Insertion of lithium into perovskite structure NbO_2F. *Mol. Cryst. Liq. Cryst. Sci. Technol., Sect. A* **1998**, *311*, 23–29.

(117) Bohnke, C.; Fourquet, J.; Randrianantoandro, N.; Brousse, T.; Crosnier, O. Electrochemical intercalation of lithium into the perovskite-type NbO_2F: influence of the NbO_2F particle size. *J. Solid State Electrochem.* **2001**, *5*, 1–7.

(118) Reddy, M.; Madhavi, S.; Rao, G. S.; Chowdari, B. Metal oxyfluorides $TiOF_2$ and NbO_2F as anodes for Li-ion batteries. *J. Power Sources* **2006**, *162*, 1312–1321.

(119) Saritha, D. Synthesis and Electrochemical Studies of ReO_3 Type Phase Nb_3O_7F. *Mechanics, Materials Science & Engineering Journal* **2018**, *14*, 1–6.

(120) Griffith, K. J.; Seymour, I. D.; Hope, M. A.; Butala, M. M.; Lamontagne, L. K.; Preefer, M. B.; Koçer, C. P.; Henkelman, G.; Morris, A. J.; Cliffe, M. J.; Dutton, S. E.; Grey, C. P. Ionic and Electronic Conduction in $TiNb_2O_7$. *J. Am. Chem. Soc.* **2019**, *141*, 16706–16725.

(121) Preefer, M. B.; Saber, M.; Wei, Q.; Bashian, N. H.; Bocarsly, J. D.; Zhang, W.; Lee, G.; Milam-Guerrero, J.; Howard, E. S.; Vincent, R. C.; Melot, B. C.; Van der Ven, A.; Seshadri, R.; Dunn, B. S. Multielectron Redox and Insulator-to-Metal Transition upon Lithium Insertion in the Fast-Charging, Wadsley-Roth Phase PNb_9O_{25}. *Chem. Mater.* **2020**, *32*, 4553–4563.

(122) Levin, E. M.; Roth, R. S. The system niobium pentoxide-phosphorus pentoxide. *J. Solid State Chem.* **1970**, *2*, 250–261.

(123) Benabbas, A.; Borel, M. M.; Grandin, A.; Leclaire, A.; Raveau, B. Redetermination of the structure of PNb_9O_{25}. *Acta Cryst.* **1991**, *C47*, 849–850.

(124) Patoux, S.; Dolle, M.; Rousse, G.; Masquelier, C. A Reversible Lithium Intercalation Process in an ReO_3-Type Structure PNb_9O_{25}. *J. Electrochem. Soc.* **2002**, *149*, A391.

(125) Koçer, C. P.; Griffith, K. J.; Grey, C. P.; Morris, A. J. Cation Disorder and Lithium Insertion Mechanism of Wadsley–Roth Crystallographic Shear Phases from First Principles. *J. Am. Chem. Soc.* **2019**, *141*, 15121–15134.

(126) Dreele, R. B. V.; Cheetham, A. K.; Anderson, J. S. The structures of some titanium-niobium oxides by powder neutron diffraction. *Proceedings of the Royal Society of London. A. Mathematical and Physical Sciences* **1974**, *338*, 311–326.

(127) Griffith, K. J.; Harada, Y.; Egusa, S.; Ribas, R. M.; Monteiro, R. S.; Von Dreele, R. B.; Cheetham, A. K.; Cava, R. J.; Grey, C. P.; Goodenough, J. B. Titanium Niobium Oxide: From Discovery to Application in Fast-Charging Lithium-Ion Batteries. *Chem. Mater.* **2021**, *33*, 4–18.

(128) Culver, S. P.; Koerver, R.; Krauskopf, T.; Zeier, W. G. Designing Ionic Conductors: The Interplay between Structural Phenomena and Interfaces in Thiophosphate-Based Solid-State Batteries. *Chem. Mater.* **2018**, *30*, 4179–4192.

For Table of Contents Only